# Selective absorption of $H_2S$ and $CO_2$ by azole based protic ionic liquids: A combined Density Functional Theory and Molecular Dynamics study

Abdul Rajjak Shaikh[1,*], Sergio Posada-Pérez[2,1], Artur Brotons-Rufes[2,1], Jason J. Pajski[3,1], Gulshan Kumar[4,1], Vajiha Hussain[5,1], Ayesha Mateen[6,1], Albert Poater[2,*], Miquel Solà[2], Mohit Chawla[7,*] Luigi Cavallo[7,*]

*[1]STEMskills Research and Education Lab Private Limited, Faridabad 121002, Haryana, India. [2]Institut de Química Computacional i Catàlisi and Departament de Química, Universitat de Girona, c/ Maria Aurèlia Capmany 69, 17003 Girona, Catalonia, Spain. [3]Department of Chemistry, East Carolina University, Greenville, North Carolina 27858, USA. [4] Department of Chemistry, MMEC, Maharishi Markandeshwar (Deemed to be University), Mullana, Haryana, India. [5]vignans foundation for science technology and research Vadlamudi, Guntur-522213, Andhra Pradesh, India. [6]Department of Clinical Laboratory Science, College of Applied Medical Science, King Saud University, Riyadh, Saudi Arabia. [7]KAUST Catalysis Center (KCC), Physical Sciences and Engineering Division (PSE), King Abdullah University of Science and Technology (KAUST), Thuwal 23955-6900, Saudi Arabia.*

**Corresponding Authors:**

Dr. Abdul Rajjak Shaikh, E-mail: ab_rajjak@yahoo.co.in

Dr. Albert Poater, E-mail: albert.poater@udg.edu

Dr. Mohit Chawla, E-mail: mohit.chawla@kaust.edu.sa

Prof Luigi Cavallo, E-mail: luigi.cavallo@kaust.edu.sa

## Highlights

1. Selective removal of $H_2S$ and $CO_2$ is essential in natural gas sweetening

2. Four azole based protic ionic liquids, viz, [DBNH][1,2,3-triaz], [DBNH][1,2,4-triaz], [DBUH][1,2,3-triaz] and [DBUH][1,2,4-triaz] were studied

3. Density functional theory and molecular dynamics simulations were carried out to understand absorption phenomenon

4. $CO_2$ binds to the nitrogen of the anion and form a C-N bond, whereas $H_2S$ generates an $HS^-$ anion

5. MD results indicate [1,2,4-triaz]- is a better anion compared to $[1,2,3\text{-triaz}]^-$

## Abstract

To achieve efficient carbon capture, utilization, and storage, it is necessary to separate $CO_2$ from the atmosphere. In an attempt to move towards selective separation of $CO_2$, some of us have shown that ionic liquids (ILs) can be efficiently used to separate $CO_2$ and $H_2S$ from $CH_4$ and $H_2O$. In the present work, we perform Density Functional Theory and Molecular dynamics simulations for four different ILs: [DBNH][1,2,3-triaz], [DBNH][1,2,4-triaz], [DBUH][1,2,3-triaz] and [DBUH][1,2,4-triaz]. DFT calculations have unveiled the additional selective character of $H_2S$ with respect to $CO_2$. Whereas $CO_2$ binds to the nitrogen of the anionic moiety of the IL forming a new C-N bond, $H_2S$ transfers a proton to one of the nitrogen atoms of the IL with the consequent generation of a $HS^-$ anion. Radial distribution function analysis shows the presence of hydrogen bonds between cation and anion in neat ILs as well in presence of gases. Hydrogen bond analysis shows higher number of hydrogen bonds in the ILs between cation and the [1,2,3-triaz] anion as compared to [1,2,4-triaz] anion. Molecular dynamics simulations also show that these ionic liquids have stronger interaction with $CO_2$ and $H_2S$ as compared to $CH_4$. Overall, our study confirms the usage of studied ILs to efficiently capture $CO_2$ and $H_2S$.

**Keywords:** $CO_2$; Azole; $H_2S$; Ionic liquids; density functional theory (DFT); molecular dynamics (MD).

## 1. Introduction

Carbon capture, utilization, and storage (CCUS) technologies to remove carbon dioxide from the atmosphere and combustion products of hydrocarbons are a topic of significant interest for nations to be able to meet their climate goals and reduce the environmental impact of anthropogenic greenhouse gases that contribute to climate change and ocean acidification. According to the World Energy Outlook 2021 report from the International Energy Agency, coal and oil use increased in 2021, with the subsequent annual increase in $CO_2$ emissions on record [1]. Efforts to reduce production of $CO_2$ alone are projected to be incapable of meeting the reduction necessary to mitigate global warming. Carbon capture is seen as a critical component of the strategy for meeting net zero emissions targets in the Paris Agreement. Materials capable of removing $CO_2$ from gas streams through physical absorption, chemical absorption, or through membranes exist but inefficiency and other problems limit their use. Diluted aqueous alkanolamines such as methanolamine are currently utilized for carbon capture, but concerns of the cost of regeneration and solvent replacement as they evaporate (creating another environmental trouble), along with their potential for oxidative degradation and reactivity with the carbon capture systems have led to search for materials with more desirable properties [2, 3].

One category of promising materials for carbon capture is ionic liquids (ILs) [4-7]. Remarkably, ILs have emerged as promising compounds for natural gas separation, solving the most common drawbacks of organic solvents, such as the generation of pollution and the high energy consumption [8-12]. The pioneering works of Blanchard and coworkers [5, 13] and Pomelly and

coworkers [14, 15], demonstrated that $CO_2$ and $H_2S$ are highly soluble in 1-butyl-3-methyl-imdazolium based compounds, boosting the research of new ILs for the capture of these undesirable gases produced during the combustion of natural gas [16, 17].

Henceforth, the $CO_2$ and $H_2S$ solubility and capture using ILs has been experimentally and theoretically investigated. For example, Jalili and coworkers determined the solubilities of both gases in a few imidazolium-based compounds, reporting the higher solubility of $H_2S$ with respect to $CO_2$ [18, 19]. Molecular simulations showed that $CO_2$ maintains the linear structure after the interaction with the tested ILs. Goel *et al*. and Hussain *et al*. investigated the $CO_2$ absorption using pyridinium ILs [20, 21] showing the bending and coordination of $CO_2$ to the anion due to N-C interaction. Balchandani and coworkers studied six different aqueous blends of hybrid solvents of 3-aminopropyl triethoxysilane, N-methyldiethanolamine, sulfolane, 1-butyl-3-methyl-imidazolium acetate activated by 1-(2-aminoethyl) piperazine, bis-(3-aminopropyl)amine, and 2-methyl piperazine [22], revealing that the activators can help to increase the solubility. Kelley *et al*. investigated the link between the formation of aromatic liquid clathrate and $CO_2$ dissolution in ILs, concluding that the use of anions with basic functional groups may improve the $CO_2$ interaction [23].

The ability of ILs to absorb gases like carbon dioxide and hydrogen sulfide make them materials of interest for carbon capture and natural gas sweetening. The low volatility of ILs compared to alkanolamines leads to much lower evaporation, decreasing the costs of solvent replacement in CCUS and reduced environmental impact. Properties of ILs are highly tunable by selection of cation-anion pairs for specific properties. One example is glycol-bonded 1,8-diazabicyclo[5.4.0]undec-7-ene ($[DBU\text{-}PEG]^{2+}$), a dication that by distributing the ion valence over a large area is able to ca. double the solubility of $CO_2$ in a mixture with

bis(trifluoromethylsulfonyl)imide ($Tf_2N^-$) as compared to that of [EMIM][$Tf_2N$] and [EMIM][$B(CN)_4$], known for their high $CO_2$ solubility [24]. Various strategies have been employed to find ILs with more desirable properties for $CO_2$ capture, including amino acid ILs (AAILs) [25-29], amine-functionalized ILs [30, 31], and phosphonium-based ILs [29, 32-34].

Another class of ILs being investigated is protic ionic liquids (PILs) [35-41]. These ILs often have a facile synthesis of a neutralization reaction achieved by stirring the acid and base together. Very recently, Zhang *et al*. selectively separated $H_2S$ and $CO_2$ from $CH_4$ in a series of azole-based PILs consisting of cations of 1,5-diazabicyclo[4,3,0] non-5-ene $[DBNH]^+$ and 1,8-diazabicyclo[5,4,0] undec-7-ene $[DBUH]^+$ in combination with the anions 1,2,4-1H-triazole $[1,2,4\text{-triaz}]^-$ and 1,2,3-1H-triazole $[1,2,3\text{-triaz}]^-$ PILs [42]. They show that the solubility of $H_2S$ is 20-30 times higher than those in conventional ILs, drastically increasing the selectivity with respect to $CH_4$. Selectivity for $H_2S$ and $CO_2$ over $CH_4$ by these PILs indicates efficacy for natural gas sweetening. Motivated by these results, here we have envisaged *ab initio* static and molecular dynamic calculations on [DBNH][triaz] and [DBUH][triaz], where triaz = [1,2,3-triaz], [1,2,4-triaz], structures displayed in Scheme 1 to systematically investigate the interaction of these protic ILs with $H_2S$, $CO_2$, $CH_4$, and $H_2O$ for CCUS applicability.

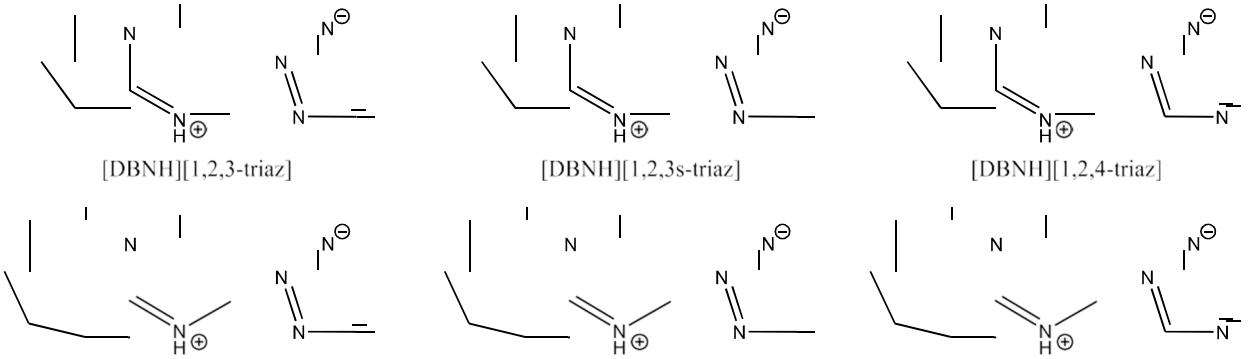

**Scheme 1**. Ionic liquids under study (s = saturated).

## 2. Computational details

### *2.1. Quantum Mechanical Calculations*

Gaussian 16 package was applied for conducting molecular modelling simulations [43]. The geometry optimizations were performed using M06-2X, *i.e.* the hybrid GGA functional of Truhlar and coworkers [44, 45], combined with the 6-311+G(d) basis set [46, 47]. The geometry optimizations were carried out without symmetry constraints, and the characterization of the stationary points was performed by analytical frequency calculations. The effect of the solvent was surveyed according to the polarizable continuum model (PCM) [48, 49], considering ethanol as the solvent.

### *2.2. Steric maps*

Steric maps and free buried volume, $\%V_{Bur}$, of the designed catalysts were obtained using the SambVca2 package of Cavallo and coworkers [50, 51].

### *2.3. Molecular Dynamics*

#### *2.3.1. Force Field Parametrization*

To simulate the cationic and anionic moieties of the IL, the Generalized Amber force field (GAFF) was used [52]. Optimized structures using Density Functional Theory (DFT) were used to fit the restrained electrostatic potential (RESP). The electrostatic potential was constructed using the Merz-Kollman method at the HF/6-31G(d) level of theory, and the electrostatic potential energy surface was generated using a multiconfigurational two-stage RESP fitting. Finally, the

Antechamber program was used to do RESP charge estimates for the cations and anionic parts of the ILs.

### *2.3.2. Molecular Dynamics Simulations for neat ILs*

The initial configurations of the IL mixture were generated by packing 2400 pairs of cations and anions using the Packmol program [53]. Molecular dynamics (MD) simulations setup is shown in Table S1. Methodology is similar to our previous articles [54-56]. All the MD simulations reported in this study was carried out using GROMACS 2019 simulation program [57]. After energy minimization, a standard protocol that includes the equilibration simulations were performed for 1 ns each using NVT and NPT ensembles. Simulated annealing was carried out to increase the temperature from 0 to 600 K. The mixture was cooled to 343 K in 50 K decrements. Further, 10 ns NPT simulation was carried out using pressure of 160 bar. Final equilibration was carried out for 10 ns using the velocity-rescaling thermostat with a coupling time of 0.1 ps and temperature of 343 K. Pressure was maintained to 1 atm, Parrinello–Rahman barostat [58] with a coupling time of 2 ps. Further, the equilibrated system was used for production simulation of 100 ns using NPT ensemble. A time step of 1 fs was used to integrate the equations of motion based on the leapfrog algorithm. The electrostatic interactions beyond 1.2 nm were evaluated for by Particle-Mesh-Ewald (PME) method [59]. In order to mimic the bulk behavior, standard Periodic boundary conditions (PBCs) in all directions were used, and the Linear Constraint Solver (LINCS) algorithm [60] was employed to constraint the hydrogen bonds.

### *2.3.3. MD simulation of ILs in presence of gases*

In addition, effect of flue gases such as $CO_2$, $CH_4$, and $H_2S$ were also studied using MD simulations by GROMACS package (Table S1). All the simulation parameters (algorithm, ensemble, step size

etc.) were similar as reported for neat ILs simulation. Analysis was carried out using Gromacs tools. Visualization was carried out using VMD program [61].

## 3. Results and discussion

### 3.1. Density Functional Theory results

Scheme 1 shows the structure of the cations and the anions used in this study. DFT calculations were first performed in order to calculate the binding energies of $CO_2$, $H_2S$, $H_2O$, and $CH_4$ with different ILs that were experimentally investigated [42], [DBNH][triaz] and [DBUH][triaz]. In addition, a newly modeled/proposed saturated [1,2,3-triaz] was also explored for the sake of comparison. In the saturated triazoles, one of the double bonds have been hydrogenated (see Scheme 1).

Starting from the analysis with [DBUH][1,2,4-triaz] (see Table 1), a thermodynamically unfavorable binding/coupling between the [DBUH][1,2,4-triaz] and $H_2O$, $H_2S$, $CO_2$, and $CH_4$ were observed with the binding energies of 2.9, 4.6, 5.5, and 8.1 kcal/mol, respectively. The calculated results seem to be in good agreement with the experimental results [42] where methane is never competitive and selectively absorbed on the studied ILs with the other studied gases/agents. Furthermore, the interaction with water (which was not studied experimentally) was investigated for a qualitative comparison of the studied gases with a relatively higher polarity. Our simulations clearly certifies that water generates a more binding effect in comparison to other studied gases. However, these results overlook an additional stabilization that would be missing for $CO_2$ and $H_2S$, as both not only have non-covalent interactions with the IL (see Figure S1 for the NCIplots, with

no significant differences with the different gases in the current study), but they modify their structure as the nitrogen in the anionic unit is able to form a covalent bond with the carbon of $CO_2$ and also to capture a proton from the $H_2S$. These two types of interactions are favorable by 3.2 and 6.0 kcal/mol, respectively, with respect to the adduct structures with simply non-covalent interactions, which are weak with respect to any covalent/ionic bond that might be formed. Nevertheless, looking at data in Table 2 one can see that after the formation of the N-C bond still the interaction is unfavorable for $CO_2$ (except for [1,2,3-triaz]$^-$ [DBUH]$^+$ and [DBNH]$^+$), whereas in agreement with experiments [42] it is favorable for $H_2S$ for the unsaturated triazoles [1,2,3-triaz]$^-$ and [1,2,4-triaz]$^-$ with both [DBUH]$^+$ and [DBNH]$^+$ cationic counterparts [62], except for the IL [DBUH][1,2,3-triaz] that is endergonic by 0.6 kcal/mol.

**Table 1**. Binding Gibbs energies (in kcal/mol) of adduct structures of the gases ($CH_4$, $H_2O$, $CO_2$, and $H_2S$) on ionic liquids (s = saturated).

| $\Delta G_{Bind}$ (ethanol) | Gas | | | |
|---|---|---|---|---|
| | $CH_4$ | $H_2O$ | $CO_2$ | $H_2S$ |
| [DBUH][1,2,3-triaz] | 8.8 | 1.4 | 7.3 | 5.8 |
| [DBUH][1,2,3s-triaz] | 8.1 | 2.0 | 6.2 | -[a] |
| [DBUH][1,2,4-triaz] | 8.1 | 2.9 | 5.5 | 4.6 |
| [DBNH][1,2,3-triaz] | 8.0 | 1.2 | 4.6 | 5.3 |
| [DBNH][1,2,3s-triaz] | 7.1 | 1.9 | 4.6 | 5.4 |
| [DBNH][1,2,4-triaz] | 7.2 | 2.5 | 5.1 | 3.6 |

[a] Complex is not formed in this case.

Moving to kinetics (see Table 2), the energy barrier of $CO_2$ insertion in [DBUH][1,2,4-triaz] would also give an indication that its absorbtion is more difficult than that of $H_2S$ by 3.7 kcal/mol (9.0 kcal/mol for $CO_2$ and 5.3 kcal/mol for $H_2S$). Looking at Table 2, similar results are obtained for the other ILs under study, pointing towards difficult absorption of $CO_2$ compared to $H_2S$. It is worth to remark that the 10.1 kcal/mol released with the saturated [1,2,3s-triaz]$^-$ must be compensated by the fact that the formation of the corresponding IL is unfavorable by exactly 10.1

kcal/mol (to be compared with the favorable values of -4.3 and -2.1 kcal/mol for [1,2,3-triaz]$^-$ and [1,2,4-triaz]$^-$, respectively), consequently making the overall process thermoneutral. The latter values is calculated from the two neutral counterparts, separately.

Focusing on the analysis of the cationic part of the ILs from [DBUH]$^+$ and [DBNH]$^+$, qualitatively there are no differences, but quantitatively. Thus, the energy barriers for the absorption of $CO_2$ increase significantly for [DBNH]$^+$ in comparison to [DBUH]$^+$. In particular, for both the [1,2,3-triaz]$^-$ and [1,2,4-triaz]$^-$ triazoles, the energy barriers increase by about 4.0 kcal/mol, but still maintaining the endergonic character of the interaction. On the other hand, for $H_2S$, the energy barriers hardly change, and a decrease in the exergonicity of the reaction is observed when going from from [DBUH]$^+$ to [DBNH]$^+$. However, for [DBNH]$^+$ the interaction with $H_2S$ is favorable for both types of triazoles, compared to [DBUH][1,2,3-triaz] that was endergonic by 0.6 kcal/mol.

To go into more detail and understand the different results obtained for [DBUH]$^+$ and [DBNH]$^+$, we analyzed the protonation capability of these two bases. The protonation of [DBN] was found to be less favorable than that of [DBU] by 1.5 kcal/mol. This explains why [DBUH]$^+$ has more $CO_2$ capture power, and obviously, even more of breaking $H_2S$, getting one of its protons. On the other hand, triazole analysis leads to much higher quantitative differences. Thus, deprotonation of [1,2,3-triaz] is 2.3 kcal/mol easier than that of [1,2,4-triaz]. It is interesting to note that the saturated conformation [1,2,3s-triaz] involves a higher cost of 17.0 kcal/mol than that [1,2,3-triaz]. And already together, the union of the two corresponding neutral units implies a stabilization of 2.1 kcal/mol by [DBUH][1,2,4-triaz] and 4.3 kcal/mol by [DBUH][1,2,3-triaz]; while the saturated form of the latter is reversed, and a disadvantageous conformation would be reached by 10.1 kcal/mol.

**Table 2**. Relative Gibbs energies (in kcal/mol) of the interaction of $CO_2$, and $H_2S$ on ionic liquids (s = saturated).

| $G_{Bind}$ (ethanol) | Gas | | | | | |
|---|---|---|---|---|---|---|
| | $CO_2$ | | | $H_2S$ | | |
| | coordination intermediate | TS | product | coordination intermediate | TS | product |
| [DBUH][1,2,3-triaz] | 7.3 | 9.2 | 6.4 | 5.8 | 5.4 | 0.6 |
| [DBUH][1,2,3s-triaz] | 6.2 | 8.2 | -10.1 | -[a] | -[a] | -10.1 |
| [DBUH][1,2,4-triaz] | 5.5 | 9.0 | 2.3 | 4.6 | 5.3 | -1.4 |
| [DBNH][1,2,3-triaz] | 4.6 | 12.8 | 2.7 | 5.3 | 5.3 | -0.9 |
| [DBNH][1,2,3s-triaz] | 4.6 | 7.6 | -12.5 | 5.4 | -[a] | -8.7 |
| [DBNH][1,2,4-triaz] | 5.1 | 12.9 | 2.9 | 3.6 | 4.0 | -0.4 |

[a] Not located in the PES.

Focusing then already the efforts with the two agents more susceptible to interact with the ILs, *i.e.* $CO_2$ and $H_2S$, to screen again if $CO_2$ thermodynamically will be or not inserted into the anionic triazole moiety, only the anionic triazole moiety was evaluated in Table 3. The coordination of $CO_2$ to $[1,2,3\text{-triaz}]^-$ leads to a destabilization of 0.8 kcal/mol, while if the saturated version is used there is a stabilization of 15.4 kcal/mol, but here it would be necessary to subtract the destabilization to form the IL first, that is, the 10.1 kcal/mol (*vide supra*), and therefore it would still be favorable by 5.3 kcal/mol. On the other hand, with $[1,2,4\text{-triaz}]^-$ there is a stabilization of 1.6 kcal/mol. Taking this into account, the cost of forming the IL from the neutral counterparts, in all the three cases, the interaction of $CO_2$ would be favorable by 3.5, 5.3 and 3.7 kcal/mol for the $[1,2,3\text{-triaz}]^-$, modeled saturated $[1,2,3s\text{-triaz}]^-$ and $[1,2,4\text{-triaz}]^-$, respectively. Thus, in all cases the $CO_2$ insertion would be feasible thermodynamically. From the IL already formed, kinetically the interaction would not be a problem as it involves a Gibbs energy barrier of 8.0, 5.1 and 7.0 kcal/mol for the triazoles $[1,2,3\text{-triaz}]^-$, modeled $[1,2,3s\text{-triaz}]^-$, and $[1,2,4\text{-triaz}]^-$, respectively. To state that before forming the C-N bond, there is a coordination intermediate, *i.e.* $CO_2$ would form a relatively unstable adduct with the IL (4-5 kcal/mol over the separated species). With $H_2S$, an

adduct is also found, almost isoenergetic with $CO_2$. But there is a difference that is, in the next step, because although the kinetic cost of the formation of the N-C bond and formation of the $HS^-$ anion is similar, thermodynamically this rupture by the triazoles releases an energy of 3.6 and 4.8 kcal/mol for the triazoles [1,2,3-triaz]$^-$ and [1,2,4-triaz]$^-$, respectively, while with the saturated [1,2,3s-triaz]$^-$, the $H_2S$ rupture is so favored that we have been able to locate neither the corresponding coordination intermediate nor the transition state. This is in agreement with the fact that with all the homologous ILs (Table 2) the transition states could not be located either, and with $[DBUH]^+$ even the initial coordination intermediate collapsed to the final product.

**Table 3**. Relative Gibbs energies (in kcal/mol) of the interaction of $CO_2$, and $H_2S$ on the anionic triazoles (s = saturated, - = not located).

| $G_{Bind}$ (ethanol) | Gas | | | | | |
|---|---|---|---|---|---|---|
| | $CO_2$ | | | $H_2S$ | | |
| | coordination intermediate | TS | product | coordination intermediate | TS | product |
| [1,2,3-triaz]$^-$ | 4.8 | 8.0 | 0.8 | 5.0 | 5.2 | -3.6 |
| [1,2,3s-triaz]$^-$ | 4.3 | 5.1 | -15.4 | -[a] | -[a] | -16.4 |
| [1,2,4-triaz]$^-$ | 4.6 | 7.0 | -1.6 | 5.0 | 5.1 | -4.8 |

[a] Not located in the PES.

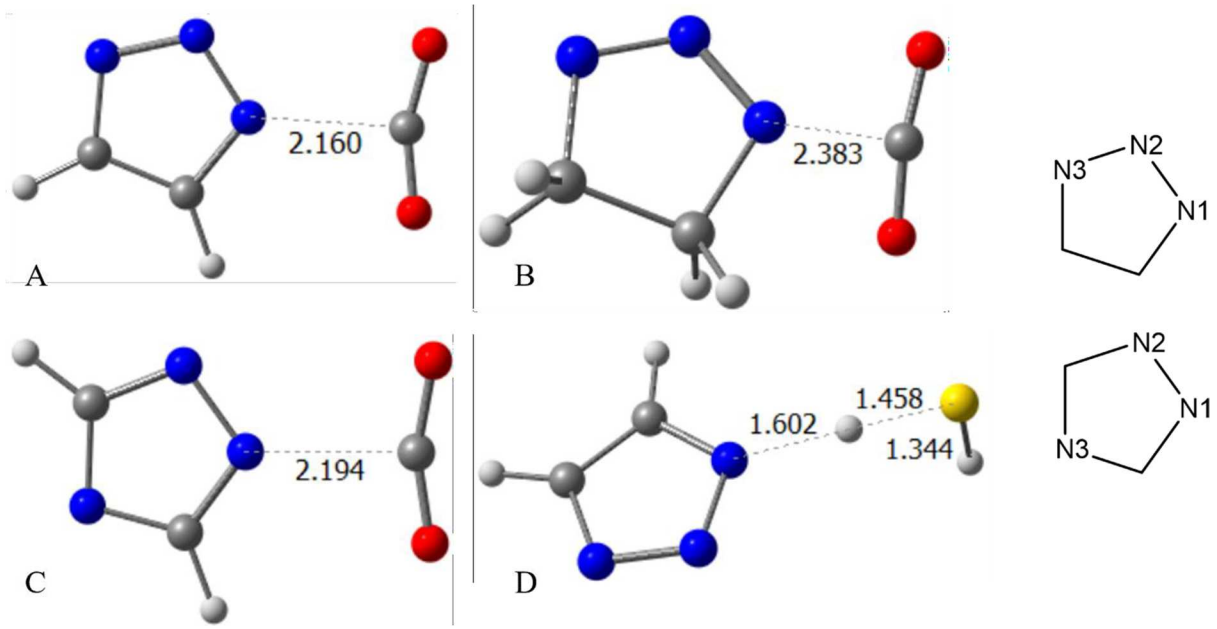


**Figure 1**. Transition states of the $CO_2$ binding for anions A: [1,2,3-triaz]$^-$ and B: [1,2,3s-triaz] [1,2,3-triaz]$^-$, C: [1,2,4-triaz]$^-$ and D: of the $H_2S$ proton transfer for [1,2,3-triaz]$^-$ (selected distances given in Å, labelling for the nitrogen atoms of the triazoles: [1,2,3-triaz]$^-$ (above) [1,2,4-triaz]$^-$ (below)).

To find out the difference between [DBUH]$^+$ and [DBNH]$^+$ when dealing with $CO_2$ the corresponding ILs with the different triazoles, steric maps in Figure 2 unveil that when the IL includes [1,2,3-triaz], before the interaction with $CO_2$, the $\%V_{Bur}$ is 44.7 % for [DBNH][1,2,3-triaz] and 49.3 % for [DBUH][1,2,3-triaz]. Whereas in the transition state of the $CO_2$ insertion the $\%V_{Bur}$ decreases from 39.0 for [DBNH][1,2,3-triaz] to 30.2 % for [DBUH][1,2,3-triaz], thus it shows the opposite behavior, comparing the two cationic moieties. This inversion comes fromthe fact that the steric hindrance of [DBNH]$^+$ is more pronounced than the one of [DBUH]$^+$ in the transition state that defines the kinetics. And this is the reason that forces that the nature of the transition state to be different. Looking at Figures 3A and 3B, it is clear that when the $CO_2$ interacts with the anionic nitrogen the protonated base does not interact with the anionic nitrogen N1, but

via the nitrogen in alpha N2. And since $[DBNH]^+$ is smaller than $[DBUH]^+$, it can tilt and it can allocate in a closer region to the entering carbon dioxide, but this means an increase of the energy barrier. On the other hand, the triazole ring $[1,2,3\text{-triaz}]^-$ in [DBUH][1,2,3-triaz] might be more nucleophilic than for [DBNH][1,2,-triaz] to facilitate the interaction with $CO_2$, but the NBO charge on N2 nearly identical, with values of -0.442 and -0.444, respectively, thus electronically the differences are not significant. Finally, the nature of the transition stated for the $H_2S$ substrate is closer to the initial coordination intermediate (see Figure 3C), but with the H-transfer from $H_2S$ to the triazole ring.

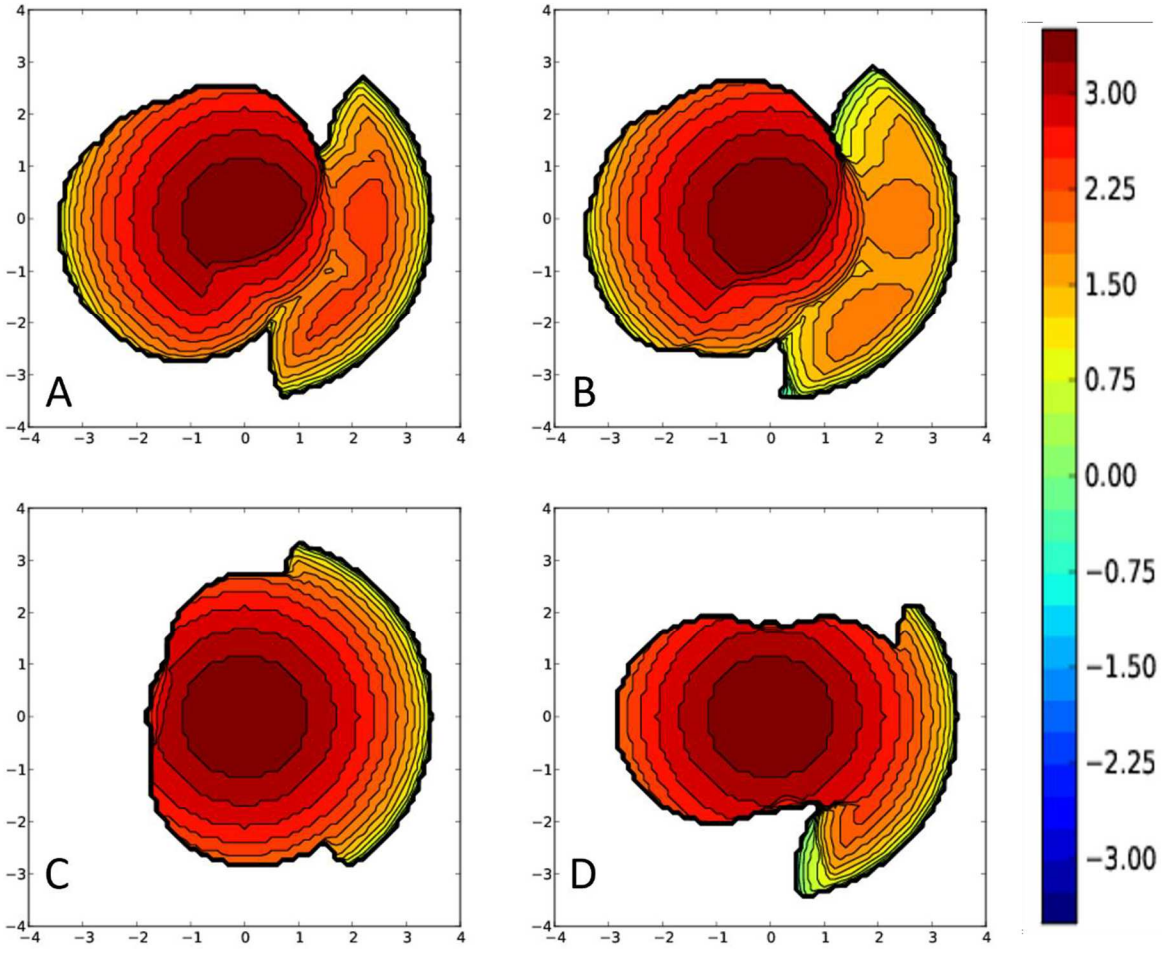

**Figure 2.** Steric maps of A: [DBNH][1,2,3-triaz], C: [DBUH][1,2,3-triaz] and for the transition state of the $CO_2$ insertion with C: [DBNH][1,2,3-triaz] and D: [DBUH][1,2,3-triaz] (xy plane, placed 2.0 Å above the plane including the linking N atom of the triazole and the N of the base that is protonated; z axis includes the carbon atom of $CO_2$; with a radius of 3.5 Å and the isocontour curves of the steric maps are given in Å).

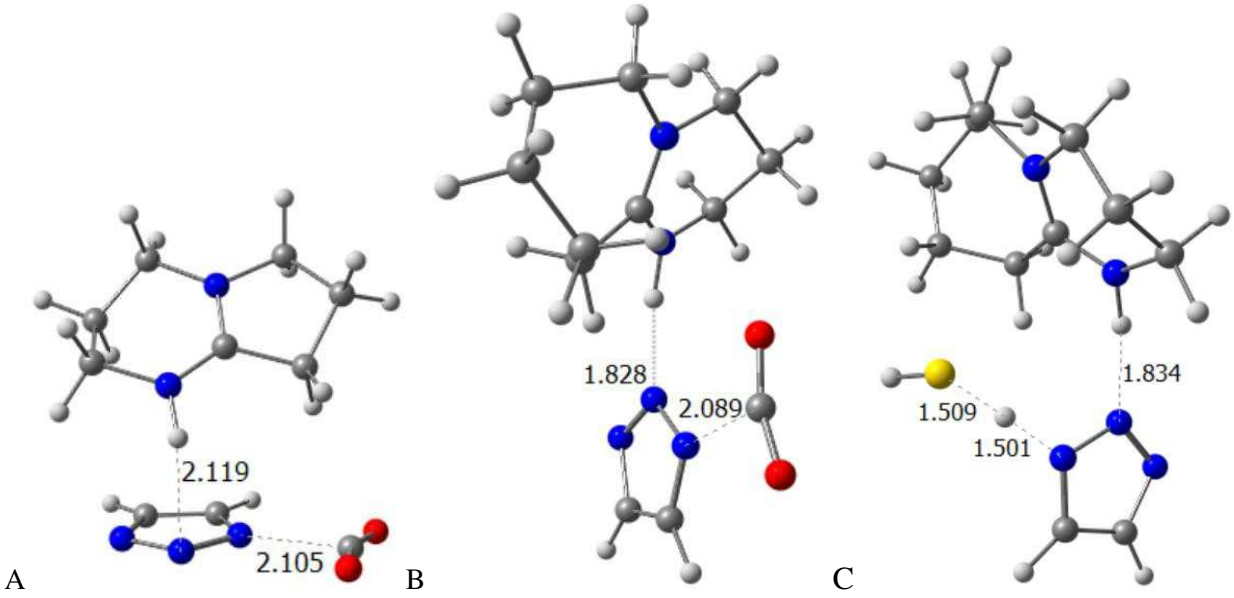


**Figure 3**. Transition states of the $CO_2$ insertion for A: [DBNH][1,2,3-triaz], B: [DBUH][1,2,3-triaz], and C: of the $H_2S$ insertion for [DBUH][1,2,3-triaz] (selected distances given in Å).

### *3.2. Molecular dynamics*

#### *3.2.1. Validation of force field:*

The chosen force−field parameters strongly impact the outcome of MD simulation, and hence, their validation is absolutely essential. One standard way available in literature for validating the

chosen force-field parameters is to compare the experimentally calculated density of molecule with the predicted density calculated by MD simulations. In this work, the prediction of densities of the neat ILs were carried out using MD simulations. Number of molecules used in MD simulation and final box size is shown in Table S1 and results corresponding to computed molecular densities from MD simulations are reported in Table 4. Remarkably, only a small difference of less than 5% has been observed between experimentally measured density [42] and predicted density using MD simulations, which clearly indicate the reliability of the chosen force field in our MD simulation studies and for the systems under investigation.

**Table 4:** Density obtained from MD simulations and experiments at 343 K of the investigated systems

| Complex | Molecular Density ($gm/cm^3$) | |
|---|---|---|
| | Simulations | Experimental[a] |
| [DBUH][1,2,3-triaz] | 1.12 ±0.3 | 1.085 |
| [DBUH][1,2,4-triaz] | 1.11 ± 0.1 | 1.095 |
| [DBNH][1,2,3-triaz] | 1.16 ± 0.4 | 1.105 |
| [DBNH][1,2,4-triaz] | 1.17 ± 0.4 | 1.115 |

[a]Experimental densities were taken from Ref. [42]

### *3.2.2. Self-Diffusion Coefficient of neat ILs and ILs in presence of flue gases*

The microscopic dynamics of ILs plays a critical role in determining the rheological properties of such compounds. The dynamics in fluids is governed by two closely related properties: atomic diffusion and viscosity. While the atomic diffusion coefficient describes single-particle diffusive transport, the viscosity describes the macroscopic transport of momentum by the collective motion

of the particles. It is well known that the self-diffusion coefficient is inversely proportional to the viscosity [63]. Self-diffusion coefficient in neat ILs is comparable in respective cations and anions of the investigated system. Further, no significant difference was observed in diffusion coefficient for cations and anion in neat ILs. In contrast, MD simulations of ILs in the presence of gases such as $CO_2$, $H_2S$, and $CH_4$ clearly revealed the notable difference in the predicted diffusion coefficients. The cation and anion in IL [DBNH][1,2,3-triaz] show relatively higher diffusion coefficient both in the case of neat ILs as well as the IL simulated in presence of different gases, see Table 5. In addition, in all the cases diffusion coefficient for $H_2S$ is higher than that of $CO_2$ and $CH_4$ in all the studied ILs, see Table 5. The trend of diffusion coefficient for gases in all ILs is $H_2S > CO_2 > CH_4$.

**Table 5.** Self-diffusion coefficients ($\times 10^{-7}$ $cm^2/s$) of the respective ions in complexes of neat ionic liquids and in presence of gases[a]

| Complex/ions | [DBNH]/[DBUH] | [1,2,3-triaz]/[1,2,4-triaz] | $[CO_2]$ | $[H_2S]$ | $[CH_4]$ |
|---|---|---|---|---|---|
| **Neat Ionic Liquids** | | | | | |
| **[DBNH][1,2,3-triaz]** | 0.03[a] | 0.01[a] | - | - | - |
| **[DBNH][1,2,4-triaz]** | 0.01[a] | 0.01[a] | - | - | - |
| **[DBUH][1,2,3-triaz]** | 0.01[a] | 0.01[a] | - | - | - |
| **[DBUH][1,2,4-triaz]** | 0.02[a] | 0.01[a] | - | - | - |
| **In presence of gases** | | | | | |

| | | | | | |
|---|---|---|---|---|---|
| **[DBNH][1,2,3-triaz]** | 6.37 ± 0.1 | 6.37 ± 0.1 | 19.39 ± 0.2 | 24.64 ± 0.2 | 10.87 ± 0.2 |
| **[DBNH][1,2,4-triaz]** | 0.33[a] | 0.29[a] | 9.28[a] | 11.81[a] | 5.70[a] |
| **[DBUH][1,2,3-triaz]** | 0.21[a] | 0.18[a] | 8.64[a] | 11.87[a] | 4.86[a] |
| **[DBUH][1,2,4-triaz]** | 0.17[a] | 0.15[a] | 6.22[a] | 8.84[a] | 5.11[a] |

[a] standard errors close to zero are not shown.

### *3.2.3. Radial Distribution Functions (RDFs) for Neat ILs*

To discuss the formation of H-bonds in ILs, RDF analysis of neat ILs was carried out considering the distance of the H atoms of the anion to the only N atom (N1) of the cation and the distance of the H atoms of the cation to three different N atoms of anion viz. N1, N2, and N3 atoms for the chosen ILs under study (see atom numbering in Figures 1 and S1). This analysis could give an indication of the structure of ILs by analyzing the distribution of ions around each other and their coordination environments. From Figures 4A and 4B, it seems evident that N1 atom of $[DBNH]^+$, does not form hydrogen bond with [1,2,3-triaz] $^-$ and $[1,2,4\text{-triaz}]^-$ which is also clear from the observed maximum peak at a distance of 0.5 nm. From Figure 4C, a sharp peak observed at a distance of 0.3 nm between N1 atom of $[DBUH]^+$ with N1 atom of $[1,2\text{-}3\text{-triaz}]^-$, clearly indicates the presence of a strong H-bonding between these two atoms. Similarly, the presence of a sharp peak at a distance of 0.3 nm in Figure 4D clearly indicates the formation of H-bonding interaction between the N1 atom of $[DBUH]^+$ with N2 atom of $[1,2,4\text{-triaz}]^-$. From the observations described above we can conclude the presence of a strong H-bonding interaction between cation $[DBUH]^+$ and anions[triaz]). In contrast, from the RDF analysis from plots (see Figure 4A, B), it is also clear

that no H-bonding interaction is present in between $[DBNH]^+$ and anions[triaz]). Finally, we also plotted the RDFs of cation-cation, cation-anion and anion-anion, and their respective coordination number, see Figure S2. As it is evident from Figure S2 for cation-anion interaction, there is a sharp solvation shell. The first largest peak for cation-anion was observed at 0.45 (0.48) nm, and the second and third peaks at 0.63 (0.62) and 1.04 (1.09) nm, for [DBNH][1,2,3-triaz] ([DBUH][1,2,3-triaz]) respectively. Similarly, in case of [DBNH][1,2,4-triaz] ([DBUH][1,2,4-triaz]), the first largest peak was observed at 0.51 (0.54) nm, and the second and third peaks at 0.63 (0.62) and 0.9 (1.13) nm respectively. Not surprisingly, it can be seen that cation-anion interaction strength seems to be higher than cation-cation and anion-anion interactions, see Figure S2. RDFs for cation-cation and anion-anion interaction shows the first peak at 0.73 nm and 0.76 nm respectively.

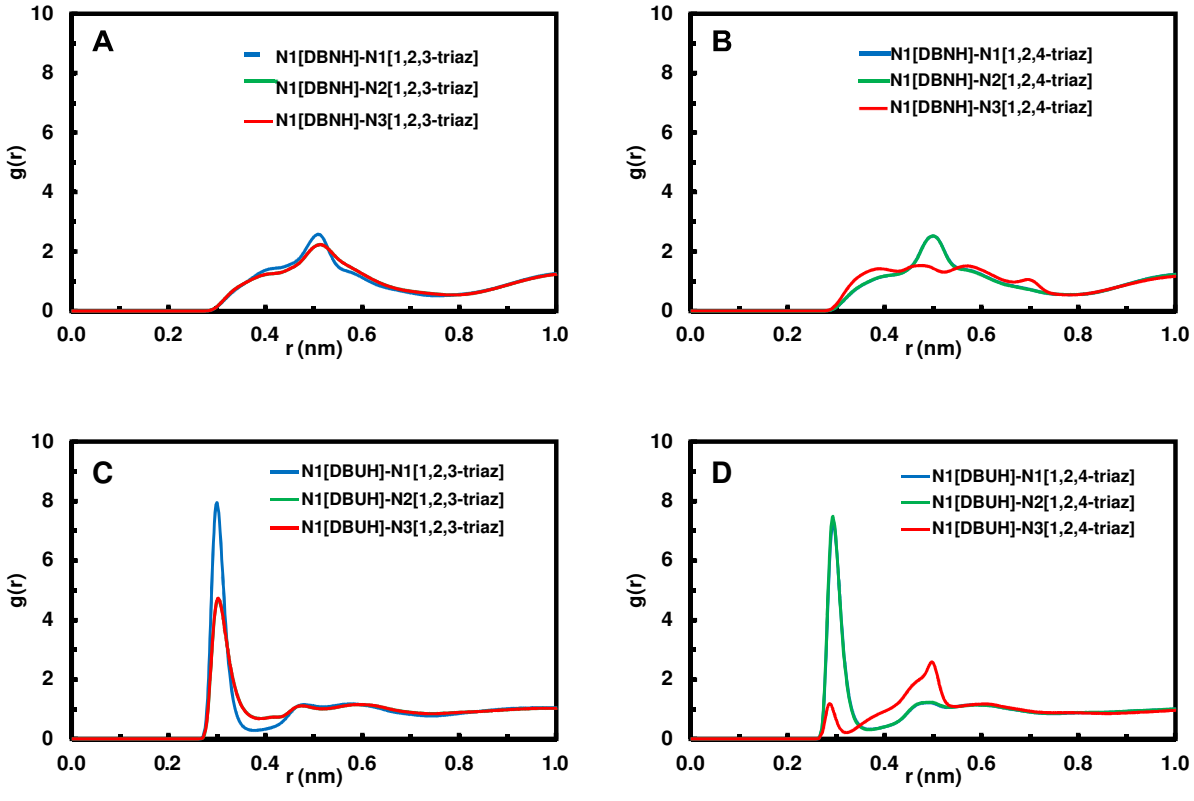


**Figure 4**. Radial distribution functions (RDFs, g(r)), indicating interionic distances between cation

and anion (r). A: RDFs for N1 atom of $[DBNH]^+$ with N1, N2 and N3 atoms of [1,2,3-triaz; B:

RDFs for N1 atom of $[DBNH]^+$ with N1, N2 and N3 atom of anion $[1,2,4\text{-triaz}]^-$; C: RDFs for N1 atom of $[DBUH]^+$ with N1, N2, N3 atoms of $[1,2\text{-}3\text{-triaz}]^-$; D: RDFs for N1 atom of $[DBNH]^+$ with N1, N2, and N3 atoms of $[1,2,4\text{-triaz}]^-$.

### *3.2.4. RDF analysis for ILs in presence of flue gases*

After adding the mixture of gases ($CO_2$, $H_2S$, and $CH_4$) in ILs, the RDFs between center of mass (COM) of cation/anion with that of O atom of $CO_2$, S atom of $H_2S$, and C atom of $CH_4$ were analyzed to study the selectivity of chosen ILs for gases under study (see Figure 5).

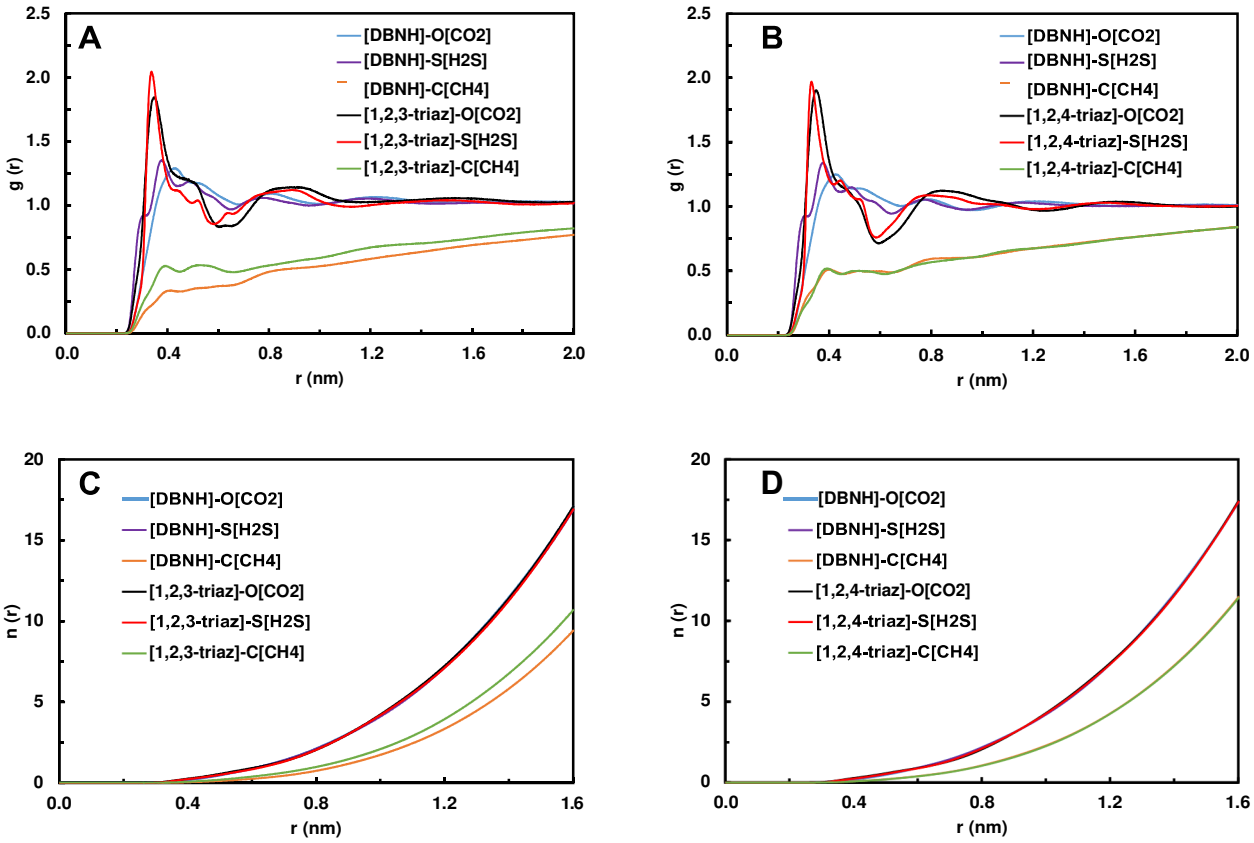


**Figure 5**. Radial distribution functions (RDFs), and their corresponding coordination numbers, indicating interionic distances between centroid of cation $[DBNH]^+$ and anion [triaz] with that of chosen atom of flue gases. Atom O is used for $CO_2$, S is used for $H_2S$ and C is used for $CH_4$ to

calculate RDFs. Centroid of cation is used in RDFs. The bottom panel (C and D) shows corresponding number integrals (n(r)) of the RDFs, which indicate the coordination numbers.

Figure 5 shows the interaction between cation/anion with $CO_2$, $H_2S$, and $CH_4$. In all the cases, based on the observed peak value of RDF, interaction between $H_2S$ and anion is highest, followed by $CO_2$. The weakest interaction was observed between $CH_4$ and the interacting cation/anion. A similar trend is observed with the interaction of gases with the cations, however, peak value is much lower as compared to anions. In case of $[DBNH]^+[1,2,3\text{-triaz}]^-$, first sharp peak is observed at 0.34 nm for interaction between$[1,2,3\text{-triaz}]^-$ and $H_2S$. Similarly, for $CO_2$, first sharp peak was observed at 0.36 nm between $[1,2,3\text{-triaz}]^-$ and $CO_2$ and in case of $CH_4$, a broad peak was observed at a distance of 0.4 nm between $[1,2,3\text{-triaz}]^-$ and $CH_4$. Finally, it is interesting to note that similar trend was observed for the interactions of $[DBUH]^+[1,2,3\text{-triaz}]^-$ with the studied $CO_2$, $H_2S$, and $CH_4$ gases as evident from the calculated RDF plots and similar peak distances between the anions and gases (Figure 6). In case of $[DBUH]^+[1,2,4\text{-triaz}]^-$, first peak was observed at 0.33 nm for interaction between $[1,2,4\text{-triaz}]^-$ and $H_2S$. Similarly, for $CO_2$, first sharp peak was observed at 0.34 nm and in case of $CH_4$, a broad peak was observed at a distance of 0.4 nm. Interaction of cation with flue gases shows RDFs in the order of $CH_4 < CO_2 \approx H_2S$.

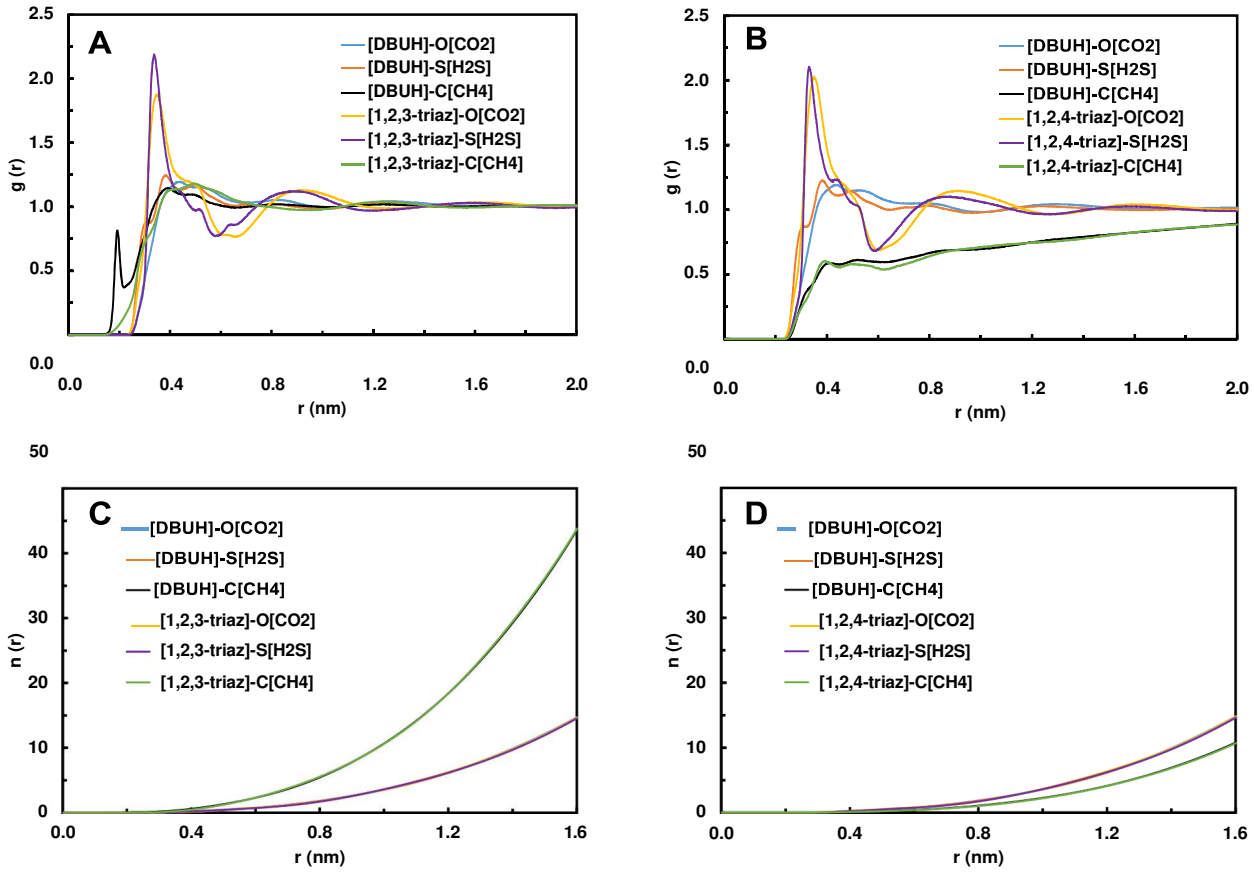


**Figure 6**. Radial distribution functions (RDFs), and their corresponding coordination numbers, indicating interionic distances between centroid of cation $[DBUH]^+$ and anion [triaz] with that of chosen atom of flue gases. Atom O is used for $CO_2$, S is used for $H_2S$ and C is used for $CH_4$ to calculate RDFs. Centroid of Cation is used in RDFs. The bottom panel (C and D) shows corresponding number integrals (n(r)) of the RDFs, which indicate the coordination numbers.

### *3.2.5. Interaction Energy of Cations and Anions in Neat ILs*

We further analyzed interaction energy between cation and anion in neat ILs and ILs in presence of gases. Total interaction energy is decomposed into two components with the first one being Coulombic component responsible for electrostatic interactions and the other one is the Lennard Jones (LJ) component which is mainly responsible for long range van der Waals interactions. Table 6 shows Coulombic and LJ interaction energy components between cation and anion in neat ILs

and in presence of gases. In neat ILs, Coulombic and LJ interaction energy is more favorable in

$[DBNH]^+[1,2,3\text{-triaz}]^-$ as compared to $[DBNH]^+[1,2,4\text{-triaz}]^-$. A similar trend was observed for $[DBUH]^+$ which shows higher interaction energy with $[1,2,3\text{-triaz}]^-$ compared to the interaction between $[DBUH]^+$ and $[1,2,4\text{-triz}]^-$. In neat ILs, not surprisingly, due to electrostatic interactions between cations and anions the calculated Coulombic component contributes to ~ >80% of calculated interaction energy component for all the studied systems and <20% contribution comes from the LJ interaction energy component.

***3.2.6. Reduction in Interaction Energy of Cations and Anions of ILs in presence of flue gases***

Looking at the interaction energy numbers from Table 6, it is clear that the overall interaction energy between cation and anion is decreased in presence of gases, except for $[DBNH]^+[1,2,4\text{-triaz}]^-$, (where the cation-anion distance is larger In case of 0.51 nm in [DBNH][1,2,4-triaz] *vs.* 0.44 nm in [DBNH][1,2,3-triaz], which may explain the lower interaction energy of [DBNH][1,2,4-triaz] in neat ILs) where the overall interaction energy component in ILs is greater in presence of mixture gases as compared to near ILs. In particular, the Coulombic component of interaction energy increases with a simultaneous decrease in LJ component of interaction energy.

One possible explanation for the reduced interaction energy between respective cation/anion pairs in neat $[DBNH]^+[1,2,4\text{-triaz}]^-$ is the due to favorable interaction of these respective cations and anions with the gases present in the system. Similar to the observations in neat ILs, the ILs in presence of gases tend to have greater interaction energy due to the favorable electrostatic component as evident from the high numbers calculated for the Coulumbic component compared to the LJ interaction energy component. While ILs in presence of gases shows favorable Coulombic interaction in [DBNH][1,2,4-triaz] as compared to $[DBNH]^+[1,2,3\text{-triaz}]^-$, LJ interaction energy is more favorable in $[DBNH]^+[1,2,3\text{-triaz}]^-$ as compared to $[DBNH]^+[1,2,4\text{-triaz}]^-$.

**Table 6.** Average interaction energy between ions in neat ionic liquids and in presence of gases.

| **Complex/ions** | **[DBNH]$^+$/[DBUH]$^+$-[1,2,3-triaz]$^-$/[1,2,4-triaz]$^-$** | | | |
|---|---|---|---|---|
| | **Coulombic (kcal/mol)** | **LJ (kcal/mol)** | **Coulombic (kcal/mol)** | **LJ (kcal/mol)** |
| | **Neat Ionic Liquids** | | **In presence of gases** | |
| **[DBNH]$^+$[1,2,3-triaz]$^-$** | -27670.92±13 | -24387.22±19 | -105164.55±96 | -20885.06±36 |
| **[DBNH]$^+$[1,2,4-triaz]$^-$** | -79939.14±23 | -22575.17±38 | -109337.60±103 | -20323.75±43 |
| **[DBUH]$^+$[1,2,3-triaz]$^-$** | -108325.41±41 | -25123.35±13 | -99268.27±98 | -21847.61±48 |
| **[DBUH]$^+$[1,2,4-triaz]$^-$** | -111606.96±103 | -23698.88±18 | -102840.93±112 | -20648.13±55 |

Table 7 shows interaction energy data for the different anions with flue gases (Table S2 contains the same values for cations). It is interesting to note that the while the LJ component of interaction energy is dominating between anion with that of $CO_2$ and $CH_4$, the coulombic interaction component is instead dominant between anion and $H_2S$. Similar trend was observed between interactions of cation with flue gases. In addition, LJ interaction component is more dominant for [DBNH]$^+$[triaz]$^-$ than for [DBUH]$^+$[triaz]$^-$ molecules.

**Table 7: Average interaction energy between anion with $CO_2$, $H_2S$ and $CH_4$**

| Complex/Anion | $CO_2$ | | $H_2S$ | | $CH_4$ | |
|---|---|---|---|---|---|---|
| | Coulombic (kcal/mol) | LJ (kcal/mol) | Coulombic (kcal/mol) | LJ (kcal/mol) | Coulombic (kcal/mol) | LJ (kcal/mol) |
| [DBNH][1,2,3-triaz] | -1110.25±3 | -2423.11±6 | -6914.75±5 | -624.71±2 | -54.41±4 | -455.81±33 |
| [DBNH][1,2,4-triaz] | -1281.41±3 | -2467.88±4 | -7703.43±8 | -459.30±1 | -71.36±4 | -509.98±31 |
| [DBUH][1,2,3-triaz] | -1154.64±4 | -2129.75±3 | -6738.53±8 | -488.60±1 | -64.67±4 | -537.04±36 |
| [DBUH][1,2,4-triaz] | -1318.57±6 | -2172.57±4 | -7291.21±3 | -355.79±1 | -82.27±5 | -595.63±36 |

### *3.2.5. Hydrogen Bond Analysis between Cations and Anions in Neat Ils and ILs in presence of flue gases*

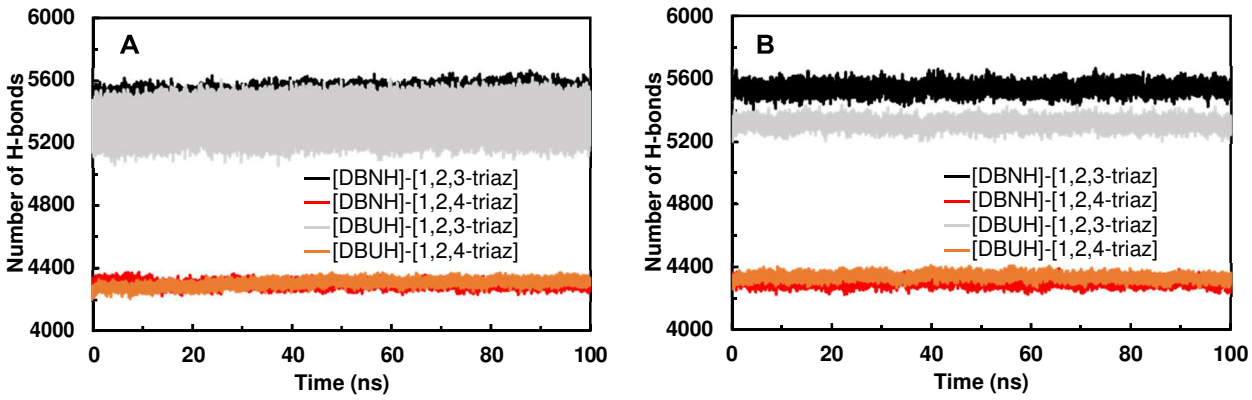


**Figure 7:** Hydrogen bond analysis between cation and anion in A: Neat ionic Liquids and in B: presence of gases.

Similar to RDFs analysis shown in Figure 6, hydrogen bond (H-bond) analysis shows more number of hydrogen bonds in $[DBNH]^+$ and $[DBUH]^+$ with $[1,2\text{-}3\text{-}triaz]^-$. H-bonds of both [DBNH] and [DBUH] cations with [1,2-4-triaz] is much lower than [1,2,3-triaz]. It is well known from literature studies that the number of H-bonds are generally connected with the viscosity of ILs [30]. Thus, from the H-bond analysis, see Figure 7 indicates that cation with $[1,2,3\text{-triaz}]^-$ could have more

viscosity as compared to ILs pairs with [1,2,4-triaz]$^-$. In other words, [DBNH]$^+$[1,2,4-triaz]$^-$ /[DBUH]$^+$[1,2,4-triaz]$^-$ is more suitable for $CO_2$ and $H_2S$ absorption as compared to [DBNH]$^+$[1,2,3-triaz]$^-$/[DBUH]$^+$[1,2,3-triaz]$^-$. The analysis of the calculated H-bonds, RDFs, self-diffusion coefficients, interaction energy analysis clearly indicates the promising absorption possessed by [DBNH][1,2,3-triaz]/[DBUH][1,2,3-triaz] ILs for both $CO_2$ and $H_2S$ thus explaining the selectivity of these gases. These results are in well agreement with the experimental findings.

## 4. Conclusions

To screen the role of simple azole based ionic liquids as fixating agents of $H_2S$ and more importantly $CO_2$ has been discussed by means of DFT calculations, as well as molecular dynamics simulations. DFT studies were able to confirm the weak interaction of $CH_4$ with the ILs, whereas the stronger interaction with the $CO_2$ and $H_2S$ adsorptions was found, which acquires higher importance for natural gas purification. In addition, the mechanism of the interaction was unveiled, finding out that for the latter gas a proton is transferred to the anion triazole. With no different electronically in terms of nucleophilicity, steric maps seem to confirm that the sterics play a clear role in the transition states the $CO_2$ insertion, which explains why the ILs with the cationic counterpart for DBN is more kinetically demanding that for DBU by roughly 3 kcal/mol for the unsaturated triazoles. MD simulation analysis revealed that the diffusion coefficients for $H_2S$ and $CO_2$ gases are greater than that of $CH_4$ in all the ILs, indicating the selectivity of ILs for $H_2S$ and $CO_2$ gases. Further, RDF analysis of ILs in presence of flue gases revealed a strong interaction between both cation and anion with $H_2S$ and $CO_2$ as compared to $CH_4$. Finally, the interaction energy between cation and anion was calculated and compared to the difference in interaction pattern after adding the gases. Overall, MD simulation Interaction energy analysis for the neat ILs

revealed that the dominant contribution of Interaction from the Coulombic component (~80%) while ~20% contribution comes from the LJ interaction energy component for all the studied systems. Further, a reduction in interaction energy of cations and anions of ILs was observed in presence of flue gases except for $[DBNH]^+[1,2,4\text{-triaz}]^-$. Finally, the H-bonding analysis points the more suitability of $[DBNH]^+[1,2,4\text{-triaz}]^-$/$[DBUH]^+[1,2,4\text{-triaz}]^-$ for $CO_2$ and $H_2S$ absorption. Overall, the analysis of the calculated self-diffusion coefficients, RDFs, interaction energy analysis and H-bonding analysis indicates the promising absorption possessed by [DBNH][1,2,4-triaz]/[DBUH][1,2,4-triaz] ILs for both $CO_2$ and $H_2S$ thus explaining the selectivity of these gases. Finally, it is interesting to note that the DFT and MD simulation results are in very well agreement with experimental data clearly indicting the usage of azole based protic ILs with $[1,2,4\text{-triaz}]^-$ as an anion shows better activity and a promising material for natural gas purification. Even though the kinetics are somewhat similar or slightly worse than for $[1,2,4\text{-triaz}]^-$, the thermodynamics are significantly better.

**CRediT authorship contribution statement**

A.R.S.: Conceptualization, Methodology, Software, Writing - original draft. A.P, S.P-P: DFT calculations and writing A.P.: DFT analysis and writing, M.S., AB-B, J.J.P, G.K, V.H., A.M., A.R.S., M.C.: Data curation, L.C.: Project administration, Resources, Supervision, M.C.: Analysis, Writing - review & editing.

**Acknowledgments**

Authors would like to thank the King Abdullah University of Science and Technology (KAUST) Supercomputing Laboratory (KSL) for providing the necessary computational resources. A.P. is a Serra Húnter Fellow and ICREA Academia Prize 2019. S.P.P thanks the Spanish Ministerio de Ciencia e Innovación for Juan de la Cierva Formación fellowship (FJC2019-039623-I). M.S. and A.P. thank the Spanish MINECO for projects PID2020-13711GB-I00 and PGC2018-097722-B-I00 and the Generalitat de Catalunya for project 2017SGR39. S.P-P., AB-R., J.J.P., G.K., V.H, A.M., thanks STEMskills Research and Education Lab Private Limited, India for providing supervision within the workshop 'MD simulations of Ionic Liquids'

## Appendix A. Supplementary material

The following are the Supplementary data to this article:

## References

[1] IEA (2021), World Energy Outlook 2021, IEA, Paris https://www.iea.org/reports/world-energy-outlook-2021. (2021).
[2] P. Luis, Use of monoethanolamine (MEA) for $CO_2$ capture in a global scenario: Consequences and alternatives. Desalination 380 (2016) 93-99.
[3] B.A. Oyenekan, G.T. Rochelle, Energy Performance of Stripper Configurations for $CO_2$ Capture by Aqueous Amines. Ind. Eng. Chem. Res. 45 (2006) 2457-2464.
[4] M. Ramdin, T.W. de Loos, T.J.H. Vlugt, State-of-the-Art of $CO_2$ Capture with Ionic Liquids. Ind. Eng. Chem. Res. 51 (2012) 8149-8177.
[5] L.A. Blanchard, D. Hancu, E.J. Beckman, J.F. Brennecke, Green processing using ionic liquids and $CO_2$. Nature 399 (1999) 28-29.
[6] J.P. Hallett, T. Welton, Room-Temperature Ionic Liquids: Solvents for Synthesis and Catalysis. Chem. Rev. 111 (2011) 3508-3576.
[7] S. Kasahara, E. Kamio, A.R. Shaikh, T. Matsuki, H. Matsuyama, Effect of the amino-group densities of functionalized ionic liquids on the facilitated transport properties for $CO_2$ separation. J. Membr. Sci. 503 (2016) 148-157.
[8] K. Friess, P. Izák, M. Kárászová, M. Pasichnyk, M. Lanč, D. Nikolaeva, P. Luis, J.C. Jansen, A Review on Ionic Liquid Gas Separation Membranes. Membranes 11 (2021).
[9] B.R. Mellein, A.M. Scurto, M.B. Shiflett, Gas solubility in ionic liquids. Curr. Opin. Green Sustain. Chem. 28 (2021) 100425.
[10] D. Shang, X. Liu, L. Bai, S. Zeng, Q. Xu, H. Gao, X. Zhang, Ionic liquids in gas separation processing. Curr. Opin. Green Sustain. Chem. 5 (2017) 74-81.

[11] S.K. Shukla, S.G. Khokarale, T.Q. Bui, J.-P.T. Mikkola, Ionic Liquids: Potential Materials for Carbon Dioxide Capture and Utilization. Front. Mater. 6 (2019) 42.
[12] X. Zhang, X. Zhang, H. Dong, Z. Zhao, S. Zhang, Y. Huang, Carbon capture with ionic liquids: overview and progress. Energy Environ. Sci. 5 (2012) 6668-6681.
[13] L.A. Blanchard, Z. Gu, J.F. Brennecke, High-Pressure Phase Behavior of Ionic Liquid/$CO_2$ Systems. J. Phys. Chem. B 105 (2001) 2437-2444.
[14] C.S. Pomelli, C. Chiappe, A. Vidis, G. Laurenczy, P.J. Dyson, Influence of the Interaction between Hydrogen Sulfide and Ionic Liquids on Solubility: Experimental and Theoretical Investigation. J. Phys. Chem. B 111 (2007) 13014-13019.
[15] C. Chiappe, C.S. Pomelli, Hydrogen Sulfide and Ionic Liquids: Absorption, Separation, and Oxidation. Top. Curr. Chem. 375 (2017) 52.
[16] S. Faramawy, T. Zaki, A.A.E. Sakr, Natural gas origin, composition, and processing: A review. J. Nat. Gas Sci. Eng. 34 (2016) 34-54.
[17] L.-y. Wang, Y.-l. Xu, Z.-d. Li, Y.-n. Wei, J.-p. Wei, $CO_2/CH_4$ and $H_2S/CO_2$ Selectivity by Ionic Liquids in Natural Gas Sweetening. Energy Fuels 32 (2018) 10-23.
[18] A.H. Jalili, M. Safavi, C. Ghotbi, A. Mehdizadeh, M. Hosseini-Jenab, V. Taghikhani, Solubility of $CO_2$, H2S, and Their Mixture in the Ionic Liquid 1-Octyl-3-methylimidazolium Bis(trifluoromethyl)sulfonylimide. J. Phys. Chem. B 116 (2012) 2758-2774.
[19] A.H. Jalili, M. Shokouhi, G. Maurer, M. Hosseini-Jenab, Solubility of $CO_2$ and $H_2S$ in the ionic liquid 1-ethyl-3-methylimidazolium tris(pentafluoroethyl)trifluorophosphate. J. Chem. Thermodyn. 67 (2013) 55-62.
[20] H. Goel, Z.W. Windom, A.A. Jackson, N. Rai, $CO_2$ sorption in triethyl(butyl)phosphonium 2-cyanopyrrolide ionic liquid via first principles simulations. J. Mol. Liq. 292 (2019) 111323.
[21] S. Hussain, H. Dong, S. Zeng, M. Umair Ahmad, F. Khurum Shehzad, H. Wu, Y. Zhang, Investigation uncovered the impact of anions on $CO_2$ absorption by low viscous ether functionalized pyridinium ionic liquids. J. Mol. Liq. 336 (2021) 116362.
[22] S.C. Balchandani, A. Dey, B. Mandal, A. Kumar, S. Dharaskar, Elucidating the important thermo physical characterization properties of amine activated hybrid novel solvents for designing post-combustion $CO_2$ capture unit. J. Mol. Liq. 355 (2022) 118919.
[23] S.P. Kelley, L.A. Flores, M.S. Shannon, J.E. Bara, R.D. Rogers, Understanding Carbon Dioxide Solubility in Ionic Liquids by Exploring the Link with Liquid Clathrate Formation. Chem. Eur. J. 23 (2017) 14332-14337.
[24] W. Shan, P.F. Fulvio, L. Kong, J.A. Schott, C.L. Do-Thanh, T. Tian, X. Hu, S.M. Mahurin, H. Xing, S. Dai, New Class of Type III Porous Liquids: A Promising Platform for Rational Adjustment of Gas Sorption Behavior. ACS Appl. Mater. Interfaces 10 (2018) 32-36.
[25] A.R. Shaikh, H. Karkhanechi, E. Kamio, T. Yoshioka, H. Matsuyama, Quantum Mechanical and Molecular Dynamics Simulations of Dual-Amino-Acid Ionic Liquids for $CO_2$ Capture. J. Phys. Chem. C 120 (2016) 27734-27745.
[26] W. Bao, Z. Wang, Y. Li, Synthesis of chiral ionic liquids from natural amino acids. J. Org. Chem. 68 (2003) 591-593.
[27] K. Fukumoto, M. Yoshizawa, H. Ohno, Room temperature ionic liquids from 20 natural amino acids. J. Am. Chem. Soc. 127 (2005) 2398-2399.
[28] H. Ohno, K. Fukumoto, Amino acid ionic liquids. Acc. Chem. Res. 40 (2007) 1122-1129.
[29] J. Zhang, S. Zhang, K. Dong, Y. Zhang, Y. Shen, X. Lv, Supported absorption of $CO_2$ by tetrabutylphosphonium amino acid ionic liquids. Chem 12 (2006) 4021-4026.
[30] K.E. Gutowski, E.J. Maginn, Amine-Functionalized Task-Specific Ionic Liquids: A Mechanistic Explanation for the Dramatic Increase in Viscosity upon Complexation with $CO_2$ from Molecular Simulation. J. Am. Chem. Soc. 130 (2008) 14690-14704.

[31] L.M. Galán Sánchez, G.W. Meindersma, A.B. de Haan, Kinetics of absorption of $CO_2$ in amino-functionalized ionic liquids. Chem. Eng. J. 166 (2011) 1104-1115.
[32] B.E. Gurkan, J.C. de la Fuente, E.M. Mindrup, L.E. Ficke, B.F. Goodrich, E.A. Price, W.F. Schneider, J.F. Brennecke, Equimolar $CO_2$ absorption by anion-functionalized ionic liquids. J. Am. Chem. Soc. 132 (2010) 2116-2117.
[33] N.D. Harper, K.D. Nizio, A.D. Hendsbee, J.D. Masuda, K.N. Robertson, L.J. Murphy, M.B. Johnson, C.C. Pye, J.A.C. Clyburne, Survey of Carbon Dioxide Capture in Phosphonium-Based Ionic Liquids and End-Capped Polyethylene Glycol Using DETA (DETA = Diethylenetriamine) as a Model Absorbent. Ind. Eng. Chem. Res. 50 (2011) 2822-2830.
[34] Y. Zhang, S. Zhang, X. Lu, Q. Zhou, W. Fan, X. Zhang, Dual amino-functionalised phosphonium ionic liquids for $CO_2$ capture. Chem 15 (2009) 3003-3011.
[35] M. Hoque, M.L. Thomas, M.S. Miran, M. Akiyama, M. Marium, K. Ueno, K. Dokko, M. Watanabe, Protic ionic liquids with primary alkylamine-derived cations: the dominance of hydrogen bonding on observed physicochemical properties. RSC Adv. 8 (2018) 9790-9794.
[36] L.E. Shmukler, I.V. Fedorova, Y.A. Fadeeva, M.S. Gruzdev, L.P. Safonova, Alkylimidazolium Protic Ionic Liquids: Structural Features and Physicochemical Properties. ChemPhysChem. 23 (2022) e202100772.
[37] I. Abdurrokhman, K. Elamin, O. Danyliv, M. Hasani, J. Swenson, A. Martinelli, Protic Ionic Liquids Based on the Alkyl-Imidazolium Cation: Effect of the Alkyl Chain Length on Structure and Dynamics. J. Phys. Chem. B 123 (2019) 4044-4054.
[38] M.A. Addicoat, R. Stefanovic, G.B. Webber, R. Atkin, A.J. Page, Assessment of the Density Functional Tight Binding Method for Protic Ionic Liquids. J. Chem. Theory Comput. 10 (2014) 4633-4643.
[39] T.L. Greaves, C.J. Drummond, Protic ionic liquids: properties and applications. Chem. Rev. 108 (2008) 206-237.
[40] C. Wang, H. Luo, D.E. Jiang, H. Li, S. Dai, Carbon dioxide capture by superbase-derived protic ionic liquids. Angew. Chem. Int. Ed. 49 (2010) 5978-5981.
[41] K. Huang, X.M. Zhang, Y. Xu, Y.T. Wu, X.B. Hu, Y. Xu, Protic Ionic Liquids for the Selective Absorption of $H_2S$ from $CO_2$: Thermodynamic Analysis. AICHE J. 60 (2014) 4232-4240.
[42] X. Zhang, W. Xiong, L. Peng, Y. Wu, X. Hu, Highly selective absorption separation of $H_2S$ and $CO_2$ from CH4 by novel azole-based protic ionic liquids. AICHE J. 66 (2020) e16936.
[43] M.J. Frisch, G.W. Trucks, H.B. Schlegel, G.E. Scuseria, M.A. Robb, J.R. Cheeseman, G. Scalmani, V. Barone, G.A. Petersson, H. Nakatsuji, X. Li, M. Caricato, A.V. Marenich, J. Bloino, B.G. Janesko, R. Gomperts, B. Mennucci, H.P. Hratchian, J.V. Ortiz, A.F. Izmaylov, J.L. Sonnenberg, Williams, F. Ding, F. Lipparini, F. Egidi, J. Goings, B. Peng, A. Petrone, T. Henderson, D. Ranasinghe, V.G. Zakrzewski, J. Gao, N. Rega, G. Zheng, W. Liang, M. Hada, M. Ehara, K. Toyota, R. Fukuda, J. Hasegawa, M. Ishida, T. Nakajima, Y. Honda, O. Kitao, H. Nakai, T. Vreven, K. Throssell, J.A. Montgomery Jr., J.E. Peralta, F. Ogliaro, M.J. Bearpark, J.J. Heyd, E.N. Brothers, K.N. Kudin, V.N. Staroverov, T.A. Keith, R. Kobayashi, J. Normand, K. Raghavachari, A.P. Rendell, J.C. Burant, S.S. Iyengar, J. Tomasi, M. Cossi, J.M. Millam, M. Klene, C. Adamo, R. Cammi, J.W. Ochterski, R.L. Martin, K. Morokuma, O. Farkas, J.B. Foresman, D.J. Fox, Gaussian 16, Revision C.01 Wallingford, CT, 2016.
[44] Y. Zhao, D.G. Truhlar, A new local density functional for main-group thermochemistry, transition metal bonding, thermochemical kinetics, and noncovalent interactions. J. Chem. Phys. 125 (2006) 194101.
[45] Y. Zhao, D.G. Truhlar, The M06 suite of density functionals for main group thermochemistry, thermochemical kinetics, noncovalent interactions, excited states, and transition elements: two new functionals and systematic testing of four M06-class functionals and 12 other functionals. Theor. Chem. Acc. 120 (2008) 215-241.
[46] A.D. McLean, G.S. Chandler, Contracted Gaussian basis sets for molecular calculations. I. Second row atoms, Z=11–18. J. Chem. Phys. 72 (1980) 5639-5648.

[47] R. Krishnan, J.S. Binkley, R. Seeger, J.A. Pople, Self‐consistent molecular orbital methods. XX. A basis set for correlated wave functions. J. Chem. Phys. 72 (1980) 650-654.
[48] V. Barone, M. Cossi, J. Tomasi, A new definition of cavities for the computation of solvation free energies by the polarizable continuum model. J. Chem. Phys. 107 (1997) 3210-3221.
[49] J. Tomasi, B. Mennucci, R. Cammi, Quantum Mechanical Continuum Solvation Models. Chem. Rev. 105 (2005) 2999-3094.
[50] L. Falivene, R. Credendino, A. Poater, A. Petta, L. Serra, R. Oliva, V. Scarano, L. Cavallo, SambVca 2. A Web Tool for Analyzing Catalytic Pockets with Topographic Steric Maps. Organometallics 35 (2016) 2286-2293.
[51] L. Falivene, Z. Cao, A. Petta, L. Serra, A. Poater, R. Oliva, V. Scarano, L. Cavallo, Towards the online computer-aided design of catalytic pockets. Nat. Chem. 11 (2019) 872-879.
[52] J. Wang, P. Cieplak, P.A. Kollman, How well does a restrained electrostatic potential (RESP) model perform in calculating conformational energies of organic and biological molecules? J. Comput. Chem. 21 (2000) 1049-1074.
[53] L. Martinez, R. Andrade, E.G. Birgin, J.M. Martinez, PACKMOL: A Package for Building Initial Configurations for Molecular Dynamics Simulations. J. Comput. Chem. 30 (2009) 2157-2164.
[54] A.R. Shaikh, M. Ashraf, T. AlMayef, M. Chawla, A. Poater, L. Cavallo, Amino acid ionic liquids as potential candidates for $CO_2$ capture: Combined density functional theory and molecular dynamics simulations. Chem. Phys. Lett. 745 (2020) 137239.
[55] A.R. Shaikh, M. Chawla, A.A. Hassan, I. Abdulazeez, O.A. Salawu, M.N. Siddiqui, S. Pervez, L. Cavallo, Adsorption of industrial dyes on functionalized and nonfunctionalized asphaltene: A combined molecular dynamics and quantum mechanics study. J. Mol. Liq. 337 (2021).
[56] A.R. Shaikh, E. Kamio, H. Takaba, H. Matsuyama, Effects of Water Concentration on the Free Volume of Amino Acid Ionic Liquids Investigated by Molecular Dynamics Simulations. J. Phys. Chem. B 119 (2015) 263-273.
[57] M.J. Abraham, T. Murtola, R. Schulz, S. Páll, J.C. Smith, B. Hess, E. Lindahl, GROMACS: High performance molecular simulations through multi-level parallelism from laptops to supercomputers. SoftwareX 1-2 (2015) 19-25.
[58] M. Parrinello, A. Rahman, Polymorphic Transitions in Single-Crystals - a New Molecular-Dynamics Method. J. Appl. Phys. 52 (1981) 7182-7190.
[59] T. Darden, D. York, L. Pedersen, Particle Mesh Ewald - an N.Log(N) Method for Ewald Sums in Large Systems. J. Chem. Phys. 98 (1993) 10089-10092.
[60] B. Hess, H. Bekker, H.J.C. Berendsen, J.G.E.M. Fraaije, LINCS: A linear constraint solver for molecular simulations. J. Comput. Chem. 18 (1997) 1463-1472.
[61] W. Humphrey, A. Dalke, K. Schulten, VMD: visual molecular dynamics. J. Mol. Graph. 14 (1996) 33-38, 27-38.
[62] S. Sadjadi, F. Koohestani, G. Pareras, M. Nekoomanesh-Haghighi, N. Bahri-Laleh, A. Poater, Combined experimental and computational study on the role of ionic liquid containing ligand in the catalytic performance of halloysite-based hydrogenation catalyst. J. Mol. Liq. 331 (2021) 115740.
[63] S.S. Moganty, R.E. Baltus, Diffusivity of Carbon Dioxide in Room-Temperature Ionic Liquids. Ind. Eng. Chem. Res. 49 (2010) 9370-9376.